ELSEVIER

European Journal of Mechanics B/Fluids 21 (2002) 341–354

EUROPEAN JOURNAL OF MECHANICS B/FLUIDS

Quasiperiodicity and chaos in the dynamics of an elastically mounted circular cylinder

Federico Domenichini

Dipartimento di Ingegneria Civile, Università di Firenze, Via Santa Marta 3, 50139 Firenze, Italy

Received 30 May 2001; received in revised form 11 October 2001; accepted 5 December 2001

Abstract

The dynamics of an elastically mounted circular cylinder immersed in an oscillating stream is investigated. The body is modelled as a two degrees of freedom purely elastic linear oscillator; the coupled body and fluid dynamics is solved numerically with a mixed spectral finite-differences method based on the vorticity-streamfunction formulation. The problem is studied assuming values of the flow parameters which ensure a two-dimensional flow and correspond to a stable periodic regime in the fixed cylinder case, the modifications of the solution when the natural frequency of the body is varied are analysed. The onset of synchronisation between vortex shedding and elastic vibrations shows the transition from periodic motion to a nonperiodic dynamics. The quasiperiodic and fully chaotic behaviour are associated to the break of symmetry of the periodic flow. The relations between the vorticity dynamics and the different regimes of body motion are analysed.

Keywords: Quasiperiodicity; Chaos; Cylinder; Viscous oscillatory flow

1. Introduction

The interaction between an oscillating stream and a cylindrical body has received a significant attention given its theoretical relevance and the pertinence of the results to problems of practical interest, among these, the design of structures like offshore platforms, heat exchangers, and suspended power cables. It also represents a prototype scheme for oscillating flow problems characterised by the presence of bluff bodies. In most cases the assumption of a rigid cylinder which is fixed, or moves with a prescribed motion, represents a good approximation of the actual fluid–structure interaction; however in several situations, take the example of a suspended cable, the flow-induced displacement can become significant and modify the geometry of the problem. The time scale of the structural response may result comparable with the forcing period, inducing synchronisation of the shedding frequency with the external one, and eventual appearance of resonance phenomena.

Notwithstanding the broad interest of the subject, the large part of the results has been obtained for the basic model, when the cylinder is assumed as fixed or its motion is externally imposed in a fluid, usually at rest, thus avoiding the analysis of the coupled fluid–cylinder interacting dynamics. In the present work, the dynamics of an elastically mounted cylinder subjected to the actions of an oscillating stream is analysed in the two-dimensional approximation. This scheme represents a model for the behaviour of a body able to develop an elastic response to the fluid actions, which is valid within the limits of acceptance of the two-dimensional fluid flow.

In the fixed cylinder case, experimental results have shown the existence of several regimes of motion. Among these, the range of existence of effectively two-dimensional regimes of motion [1,2], the appearance of three-dimensional instabilities [3], the viscous–turbulent transition of the separated wake [4] have been determined depending on the values of the dimensionless parameters governing the problem. Several different possible flow configurations are found even within the range of two-

E-mail address: federico@ingfi1.ing.unifi.it (F. Domenichini).

0997-7546/02/$ – see front matter
PII: S0997-7546(01)01179-7

dimensional flow, these are characterised by a different evolution of the boundary-layer and of the vorticity separated from the cylinder surface; the dynamics of vortices has been related to the forces acting on the body, whose estimation represents a primary objective for applied results. In this perspective, a large amount of work has been devoted to the synthetic description of the forces from the available data, quantifying the coefficients of the well-known Morison's equation.

The complex dynamics given by the superposition of an external stream and a prescribed body motion has also been analysed [5], showing a variety of vorticity patterns; these studies are focussed on the interaction between the stream-induced wake and the forced vibration while they do not consider the actual fluid-body interaction. The coupled dynamics has been analysed in the case of the in-line response of an elastically constrained cylinder subjected to an oscillating stream [6]. Although the cylinder motion is there limited to a one degree of freedom, the study shows the presence of a strong mutual influence between the body motion and the flow evolution.

In the present work we analyse the two-dimensional coupled dynamics of an elastically mounted circular cylinder and an oscillating sinusoidal stream. The body is constrained by a pair of linear springs, acting in the coordinate directions, the cylinder-springs system is therefore a two degrees of freedom linear oscillator. Such a scheme represents a first step in modelling the actual interaction between an external forcing and a moving body; the choice of linear springs has shown to be necessary in a first study to avoid a further unpredictability present in nonlinear oscillators. The structural damping is neglected in order to avoid the need to identify the role of different smoothing phenomena, and to reduce of the number of free parameters. The present elastic problem, when the body does not start to move transversely, can be compared with the oscillating cylinder results by Anagnostopoulos and Iliadis [6] in their limit cases characterised by small levels of damping. In this study the onset of synchronisation between shedding and elastic vibrations is studied in details: the transition from periodic motion, when the frequencies of the external stream and the natural elastic fluctuations are essentially independent, to resonant possibly nonperiodic dynamics is analysed; the relation between wake dynamics, i.e. the dynamics of vortex structures, and the fluctuations of forces acting on the body is sought.

The two-dimensional assumption does not allow a description of three-dimensional flow instability phenomena [2–4,7–9]. Therefore, the problem has been analysed for values of the flow parameters well inside the range of validity of the two-dimensional approximation in the fixed cylinder case. Significant cylinder displacements may modify the conditions of stability and possibly not guarantee a two-dimensional problem. In such cases the present analysis would not furnish a complete description of the actual flow evolution, nevertheless it can be considered that the onset of the instability does not modify substantially the essential features of the flow evolution, as pointed out by several authors [9–11]. On the contrary, it is shown here that the unsteady behaviour is sometimes associated with small frequency fluctuations and long transitory before reaching the unsteady regime conditions. These effects require very long integration times, to get experimentally comparable conditions, which are not currently feasible with accurate three-dimensional integration.

The problem is studied at fixed values of the flow parameters with varying the natural frequency of the oscillator. The system is simulated by the numerical integration of the Navier–Stokes equations, in the vorticity-streamfunction formulation, written in a reference system moving with the cylinder. The fluid equations are solved simultaneously with the cylinder equations of motion. A brief description of the mathematical formulation and numerical method is reported in Section 2, the results are described and discussed in Section 3, conclusions are then summarised in Section 4.

2. Mathematical formulation and numerical method

In the present work we consider an elastically mounted circular cylinder of radius R subjected to the actions of a two-dimensional flow of an incompressible viscous fluid with density ρ and kinematic viscosity ν. The undisturbed velocity of the fluid in the x^* direction is $U^*_\infty(t^*) = U_0 \sin(2\pi t^*/T)$, t^* is the time. The cylinder motion is constrained by two linear springs, acting in the coordinate directions; the system is, therefore, characterised by the cylinder mass per unit length $M^* = \rho_c \pi R^2$, ρ_c is the body density, and by the stiffness coefficients of the springs, here assumed of equal strength with elastic constant K^*; the natural frequency of the cylinder therefore can be written $f^*_c = (K^*/M^*)^{1/2}/2\pi$. The problem can be made dimensionless choosing the radius R, the maximum external velocity U_0, and ρR^2 as unit length, velocity, and mass per unit length, respectively. An exception is used for the dimensionless time which is defined as $t = t^*/T$ in order to have a constant unitary period for the external forcing In what follows dimensionless quantities are considered unless otherwise stated.

The body motion can be described in the dimensionless Cartesian system of coordinates $\{x, y\}$, with the position of its centre $\{x_c, y_c\}$. It is convenient to use a new system of coordinates $\{\xi, \zeta\}$, moving with the cylinder; it is related to the fixed one by $\xi = x - x_c(t)$, $\zeta = y - y_c(t)$, giving for the velocity $u_\xi = u_x - U_c(t)$, $u_\zeta = u_y - V_c(t)$, where (U_c, V_c) is the cylinder velocity. Formally, the Navier–Stokes equations, rewritten in the new system of coordinates, are not modified if we introduce a scalar field $\widehat{p}(\xi, \zeta) = p(\xi, \zeta) + (\mathrm{d}U_c/\mathrm{d}t)\xi + (\mathrm{d}V_c/\mathrm{d}t)\zeta$, where p is the actual pressure distribution [12]; the boundary conditions of the problem must be modified accordingly. The Navier–Stokes equations are written in the vorticity-streamfunction formulation in the polar system of coordinates $\{r, \theta\}$, moving with the body. The equations to be solved are

$$\frac{1}{KC}\frac{\partial\omega}{\partial t}=\frac{1}{r}\left(\frac{\partial\psi}{\partial r}\frac{\partial\omega}{\partial\theta}-\frac{\partial\psi}{\partial\theta}\frac{\partial\omega}{\partial r}\right)+\frac{1}{Re}\nabla^2\omega, \tag{1}$$

$$\nabla^2\psi=-\omega, \tag{2}$$

$KC=U_0T/2R$, $Re=2U_0R/\nu$ are the Keulegan–Carpenter and the Reynolds number, respectively. An alternative form of Eq. (1) can be written using the Stokes parameter $\beta=Re/KC=4R^2/\nu T$ in place of the Reynolds number. From a computational point a view, it is convenient to introduce a stretched coordinate in the radial direction $\eta=\ln(r-1+a)-\ln(a)$, which ensures a better resolution close to the cylinder wall, a is the stretching parameter. Far from the cylinder the flow is irrotational; assuming the instantaneous velocity of the cylinder as known, the streamfunction in the moving coordinate system can be written as

$$\psi_0(r,\theta)=-\frac{1}{2}\left([V_\zeta+\mathrm{i}U_\xi]\mathrm{e}^{\mathrm{i}\theta}+[V_\zeta-\mathrm{i}U_\xi]e^{-\mathrm{i}\theta}\right)\left(r-\frac{1}{r}\right), \tag{3}$$

being $U_\xi=U_\infty-U_c$, $V_\zeta=-V_c$, i is the imaginary unit. It is convenient to split the solution in two contributions, namely $\psi=\psi_0+\phi$, with the latter term describing the rotational part of the flow. The equations of motion must be completed with the boundary conditions. Far from the cylinder, both the vorticity field and rotational term of the streamfunction must vanish. At the body surface, the no-slip condition can be written using the streamfunction derivatives, giving $\partial\phi/\partial\theta=0$ and $\partial\phi/\partial\eta=-\partial\psi_0/\partial\eta$. The azimuthal periodicity of the problem suggests a spectral representation in the θ-direction, writing any function f involved in the problem as $f(r,\theta)=\sum f_n(r)\mathrm{e}^{\mathrm{i}n\theta}$, the reality of the physical quantities implies $f_n=f^*_{-n}$, with the star denoting complex conjugate. The substitution of the spectral representation into (1) and (2) leads to a simpler problem for any term of the expansion, which is completed with the appropriate boundary conditions. The conditions on the streamfunction value at the body surface are used to solve the Poisson equations, while the conditions on its derivatives are used to derive the vorticity field, as a standard procedure [13]. At $t=0$ the flow is assumed to be irrotational.

So far, the cylinder motion has been considered as known, while it is due to the actions of the fluid and to the elastic force of the constraints. The cylinder parameters are its dimensionless mass $M=\pi\rho_c/\rho$ and the stiffness coefficients of the spring $K=K^*/\rho U_0^2$. The equation of motion of the cylinder can be written in compact form as

$$\frac{M}{KC^2}\frac{\mathrm{d}}{\mathrm{d}t^2}\begin{pmatrix}x_c\\y_c\end{pmatrix}+K\begin{pmatrix}x_c\\y_c\end{pmatrix}=\begin{pmatrix}F_x\\F_y\end{pmatrix}. \tag{4}$$

The forcing terms in Eqs. (4) are evaluated by analytical integration along the cylinder surface of the pressure and shear stress distribution. At the body surface, we have the tangential stress $\tau_{r\theta}=2\omega/Re$. The θ-component of the Navier–Stokes equations gives for the pseudo-pressure $\partial\widehat{p}/\partial\theta=(2/aRe)\partial\omega/\partial\eta$; this relationship can be integrated along the cylinder surface, furnishing the spectral representation of the pressure field at the wall. Thus, integrating again along the body surface and subtracting the inertial terms due to the change of the reference system, we obtain

$$F_x=\frac{\mathrm{i}2\pi}{Re}\left(\omega_{-1}-\omega_1-\frac{1}{a}\frac{\partial(\omega_{-1}-\omega_1)}{\partial\eta}\right)+\frac{\pi}{2KC}\frac{\mathrm{d}U_c}{\mathrm{d}t}, \tag{5a}$$

$$F_y=\frac{2\pi}{Re}\left(\omega_{-1}+\omega_1-\frac{1}{a}\frac{\partial(\omega_{-1}+\omega_1)}{\partial\eta}\right)+\frac{\pi}{2KC}\frac{\mathrm{d}V_c}{\mathrm{d}t}, \tag{5b}$$

being the vorticity and its derivative evaluated at $r=1$, or $\eta=0$. The problem must be completed imposing the condition at $t=0$; in what follows, the cylinder initially at rest is placed at the origin of the fixed system of coordinates.

The equations of the fluid motion are numerically integrated using a mixed spectral finite-difference method and an explicit time marching scheme. At each time level, the derivative of the nth term of the expansion $\partial\omega_n/\partial t$ is computed. Then, the vorticity field is advanced in time using a low-storage third-order Runge–Kutta scheme [14]. The radial space derivative are made discrete using centred second-order finite differences. The nonlinear term is evaluated in the physical space using a pseudospectral method; aliasing has been removed by the zero-padding technique. An alternative version of the numerical code with aliasing removal by phase shifts has been also implemented, showing indistinguishable results and a slightly lower computational efficiency [15]. Once ω_n has been evaluated, the discrete form of the Poisson equation leads to two linear tridiagonal system of N_r equations with diagonal dominance, being N_r the number of points in the r-direction, which are solved by using a standard method; afterwards, the wall vorticity is updated using the known conditions at the cylinder surface. At each substep of the Runge–Kutta method, the forces acting on the cylinder are evaluated (5), and the cylinder motion is updated integrating Eq. (4). The boundary conditions at infinity are imposed at a large, but finite, distance $r_{\max}$, defining the computational domain in the radial direction. In what follows, a value of $r_{\max}=100$ has been adopted; a typical stretching parameter is $a=0.4$. The numerical simulations has been performed with N_r ranging between 128 and 256, and a number N_θ of modes in θ-direction varying between 64 and 128. The time step has been chosen in order to satisfy the convective and diffusive stability conditions [13]. The perturbation of the numerical symmetry of the flow is achieved rotating the cylinder

during the first period of the external stream [10]. Preliminary tests have been performed to check the numerical code in several cases and in sensibly different conditions [16].

3. Results

In what follows, the problem has been studied fixing $KC = 1$ and $Re = 196$ ($\beta = 196$); these values correspond to a periodic and symmetric solution in the fixed cylinder case [2,10]. The dimensionless cylinder mass has been assumed equal to 24, approximately corresponding to a steel body immersed in water; the problem has been therefore analysed varying the stiffness K of the springs, thus the natural frequency $f_c = KC(K/M)^{1/2}/2\pi$. The added mass contribution acts diminishing such a frequency to a lower value $f_{c'}$. The values of $f_{c'}$ reported in what follows have been estimated a posteriori from the numerical results: the spectral analysis have been performed taking different lengths of the signal, evaluating the reduced frequency. The frequency f_c has been varied in the range 0.05–3, corresponding to reduced frequencies $f_{c'}$ between 0.047 and 2.81, to be compared with the frequency of the external stream $f_0 = 1$.

Far from the resonance condition, the system shows a solution which is periodic in time and symmetric in space (with the x-axis as the symmetry axis). The boundary-layer which develops at the cylinder surface during the accelerating phases does not separate and remains attached even during the following deceleration. The dynamics resembles that of the fixed body case at the same value of the β parameter and at low KC numbers [2,10]. As an example, the instantaneous vorticity fields at $t = 199$ and $t = 199.5$ are reported in the upper half of Fig. 1, $f_{c'} = 1.167$, showing the symmetry and the periodicity of the flow evolution. The vorticity evolution induces a periodic in-line motion of the cylinder and damped y-oscillations after the initial perturbation. The final sinusoidal motion of the body after 200 periods of calculation is reported in the lower half of Fig. 1 for several values of $f_{c'}$. The cylinder characteristics influence the solution in terms of oscillation amplitude; small

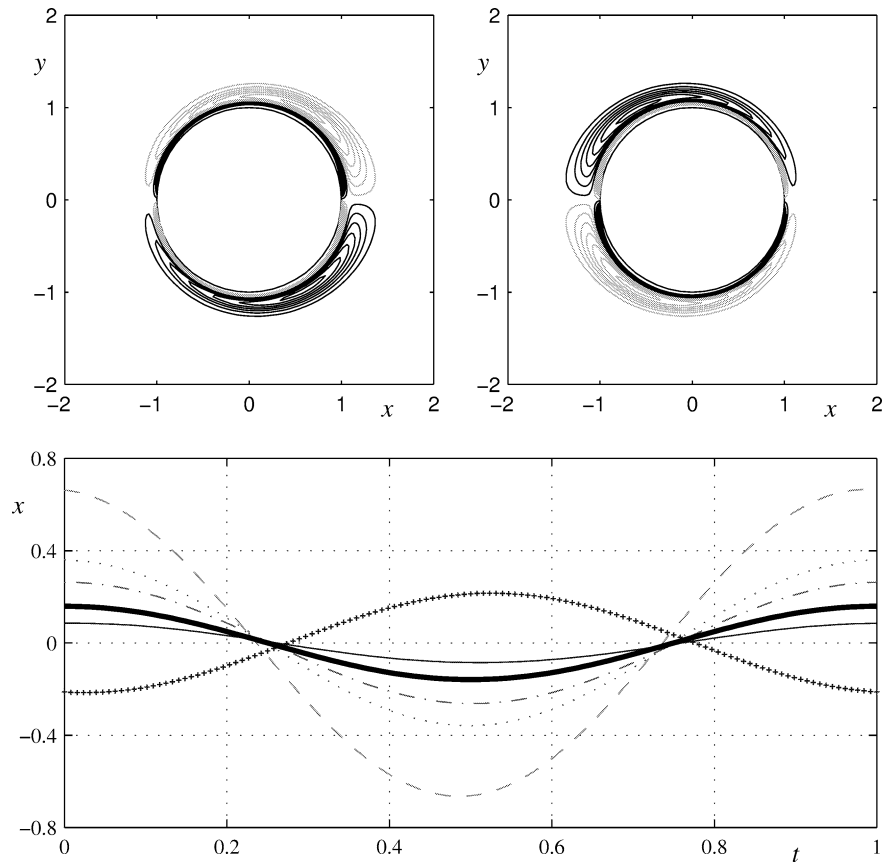

Fig. 1. Instantaneous vorticity fields, $f_{c'} = 1.167$ (upper half); contour levels from 0.5 to 10.5 with step 1 (black), and symmetric negative values (grey). Lower half: x-motion of the cylinder; $f_{c'} = 0.46$ (solid line), 0.837 (dash-dotted line), 0.887 (dotted line), 0.941 (dashed line), 1.167 (+). The thick line represents the oscillation of the undisturbed stream.

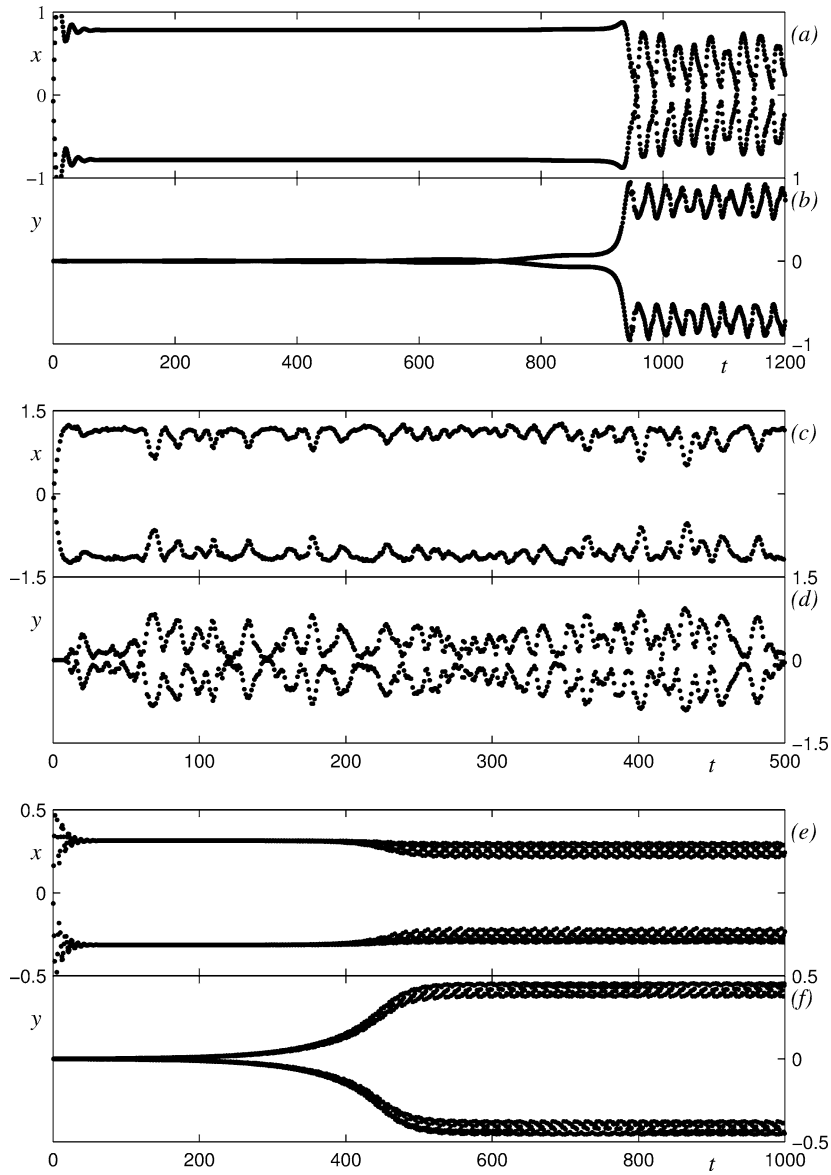

Fig. 2. Maximum cylinder displacement in each period of the external stream: $f_{c'} = 0.954$, (a) x-component, (b) y-component; $f_{c'} = 1.035$, (c) x-component, (d) y-component; $f_{c'} = 1.133$, (e) x-component, (f) y-component.

phase differences between the body motion and the imposed external stream have been detected for $f_{c'} < 1$, while an almost opposition in phase for $f_{c'} > 1$ [6]. In the analysed periodic cases the relative velocity U_ξ ranges between 0.2 and 1.6; thus the actual Keulegan–Carpenter number relative to the body corresponds to the regular solutions [2,10].

When the cylinder is fixed, higher *KC* numbers are related to the loss of symmetry of the flow field, accompanied by significant forces in the y-direction; these correspond to different regimes of motion, different dynamics of the separated wake vorticity [1,2]. A separation of the wake and a role for vortex structures is expected in the present case when the resonance condition is approached, when the growth of the cylinder in-line velocity leads to the growth of the effective *KC* number relative to the body. Data from three solutions near the resonant condition are reported in Fig. 2; the maxima, positive and negative, displacements of the body detected during each period of the external stream are plotted for three values of $f_{c'}$.

The cylinder displacements near the resonance when $f_{c'} = 0.954$ is shown in Figs. 2(a) and 2(b), this is the smallest analysed value which gives a nonperiodic solution. After the initial perturbation, the x-motion presents an approximately periodic evolution and the transversal body displacement has a slowly growing exponential behaviour. At $t \simeq 950$, an almost abrupt

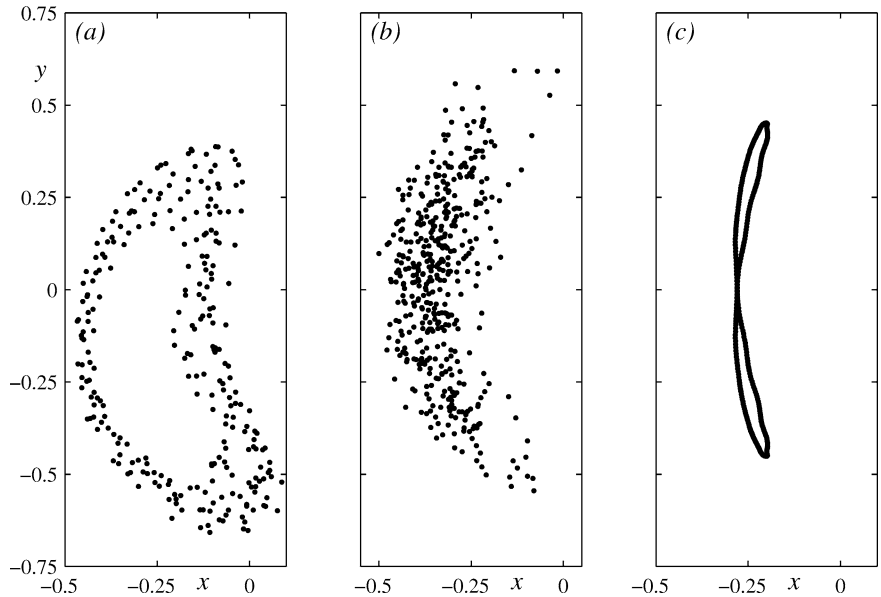

Fig. 3. Poincaré maps of the cylinder trajectory: (a) $f_{c'} = 0.954$, (b) $f_{c'} = 1.035$, (c) $f_{c'} = 1.133$.

growth of the y-displacement can be observed, with the contemporarily complete loss of periodicity of the solution, Fig. 2(a). During a significantly long period, say $t < 500$, the flow does not give any significant indicator of such a subsequent transition, the y-oscillations have an amplitude several orders of magnitude smaller than the in-line one. This extremely weak instability, and the following abrupt transition, suggests particular care when taking conclusions after a limited period of observation in analogous conditions. This specific case does represent a singular condition in the boundary with periodic regime. The same behaviour has been found at higher values of the proper frequency, $f_{c'} = 0.963$ and $f_{c'} = 0.965$, with the anticipated appearance of the abrupt transition, at $t \simeq 450$ and $t \simeq 150$, respectively. On the opposite, $f_{c'} = 0.945$ gives a stable periodic solution, with a damped y-motion after the initial perturbation. The periodic–chaotic transition is therefore contained in the narrow range 0.945–0.954, it is characterised by a weak instability of the periodic and symmetric solution which appears after a such long period of evolution that prevents from a more detailed analysis. A different evolution has been observed in a range about the resonance. The solution in correspondence of $f_{c'} = 1.035$, Figs. 2(c) and 2(d), presents a larger amplitude of the x-motion which modifies the vorticity dynamics with an almost instantaneous loss of symmetry and a rapid development of the y-motion. The presence of several vortices close to the body and their interaction with the boundary-layer at the cylinder surface gives the observed chaotic behaviour. A different transition to the chaotic regime has been detected when $f_{c'}$ decreases from values larger than one: the periodic and chaotic regimes are separated by a well defined range corresponding to a quasiperiodic solutions. In Figs. 2(e) and 2(f) the cylinder quasiperiodic motion is plotted at $f_{c'} = 1.133$, where also the confirmation for the necessity of long-time analyses is evident.

The characteristics of the solutions suggested by Fig. 2 can be better recognised from the Poincaré maps of the cylinder trajectory, Fig. 3; the unitary period of the external stream is the sampling time interval, the plotted points correspond to the last 270, 450, and 400 computed periods, respectively. The comparison of the maps clarify the differences between the solutions, showing a weakly chaotic behaviour at $f_{c'} = 0.954$, Fig. 3(a), a completely chaotic one at $f_{c'} = 1.035$, Fig. 3(b); the quasiperiodicity of the cylinder motion at $f_{c'} = 1.133$ can be depicted from Fig. 3(c), where the plotted points define a closed curve.

Such a classification is also confirmed by the spectral analysis. In the periodic cases, the spectra of the x-quantities are characterised by an isolated peak at the unitary external frequency f_0, and the y-motion by the contribution at the body proper frequency $f_{c'}$. Nonperiodic regimes present spectra with different important features that are here briefly summarised. In the case $f_{c'} = 0.954$, which represents the periodic–chaotic transition for $f_{c'} < 1$, the x-motion shows a sensible decrease of the fundamental contribution at $f_0 = 1$, with the appearance of two additional ones, at the natural frequency $f_{c'}$ and at $f_1 = 2 - f_{c'}$, Fig. 4(a) where the amplitude spectrum S_x of the in-line motion is reported. The spectrum S_y of the y-component presents a similar behaviour, with the dominance of the unitary external frequency, Fig. 4(b). The spectra corresponding to the chaotic regime close to the resonance condition, $f_{c'} = 1.035$, are reported in Figs. 4(c) and 4(d). This case is characterised by the significant growth of the x-motion, the contribution at the fundamental frequency is dominant, while additional peaks are not recognisable, Fig. 4(c). A more broad-band spectrum S_y can be observed in Fig. 4(d), where several contributions close

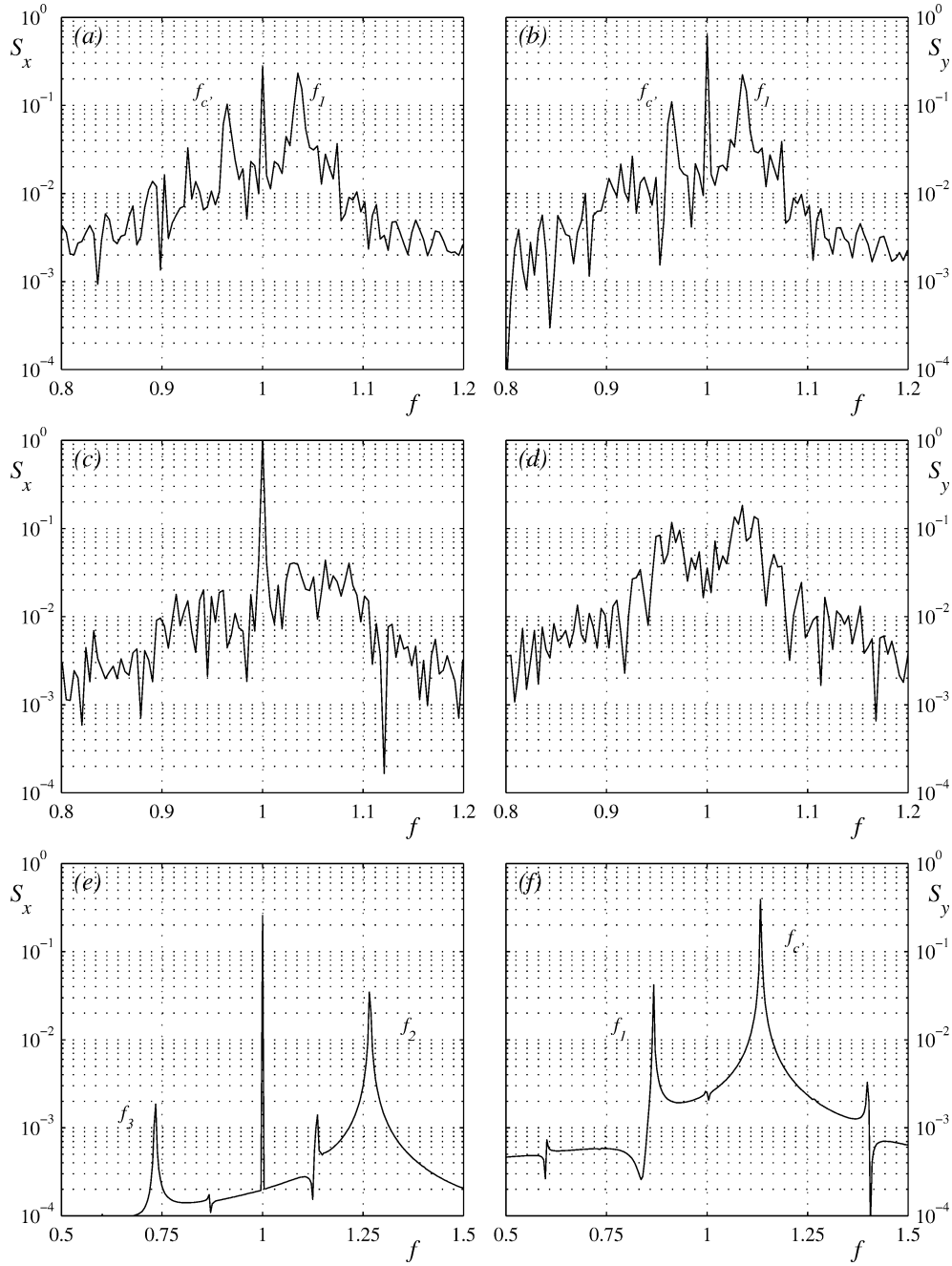

Fig. 4. Amplitude spectra of the cylinder displacements: $f_{c'} = 0.954$, (a) S_x, (b) S_y; $f_{c'} = 1.035$, (c) S_x, (d) S_y; $f_{c'} = 1.133$, (e) S_x, (f) S_y.

to $f_{c'}$ and f_1 become significant. When $f_{c'}$ is in the quasiperiodic range 1.129–1.137, i.e. f_c between 1.1875 and 1.2, the transversal motion is greater than the in-line one. The spectrum S_x in the case $f_{c'} = 1.133$ shows two well recognisable additional contributions, a primary at $f_2 = 2f_{c'} - 1$ and a secondary one at $f_3 = 3 - 2f_{c'}$. The contribution at f_2 appears however as a modulating effect, being approximately 1/10 of the fundamental one, Fig. 4(e). The y-motion is dominated by the reduced natural frequency with a modulation at f_1, Fig. 4(f). A smaller frequency, $f_c = 1.16$ or $f_{c'} \simeq 1.109$, gives a weakly chaotic solution, whereas a further decrease of $f_{c'}$ leads to the chaotic regime reported in Figs. 4(c) and 4(d).

The dependence of the solution on the cylinder frequency is summarised in Fig. 5. The estimation of the reduced frequency $f_{c'}$ permits an evaluation of the inertial coefficient $C_i = M((f_c/f_{c'})^2 - 1)/\pi$, Fig. 5(a). The values of C_i are substantially

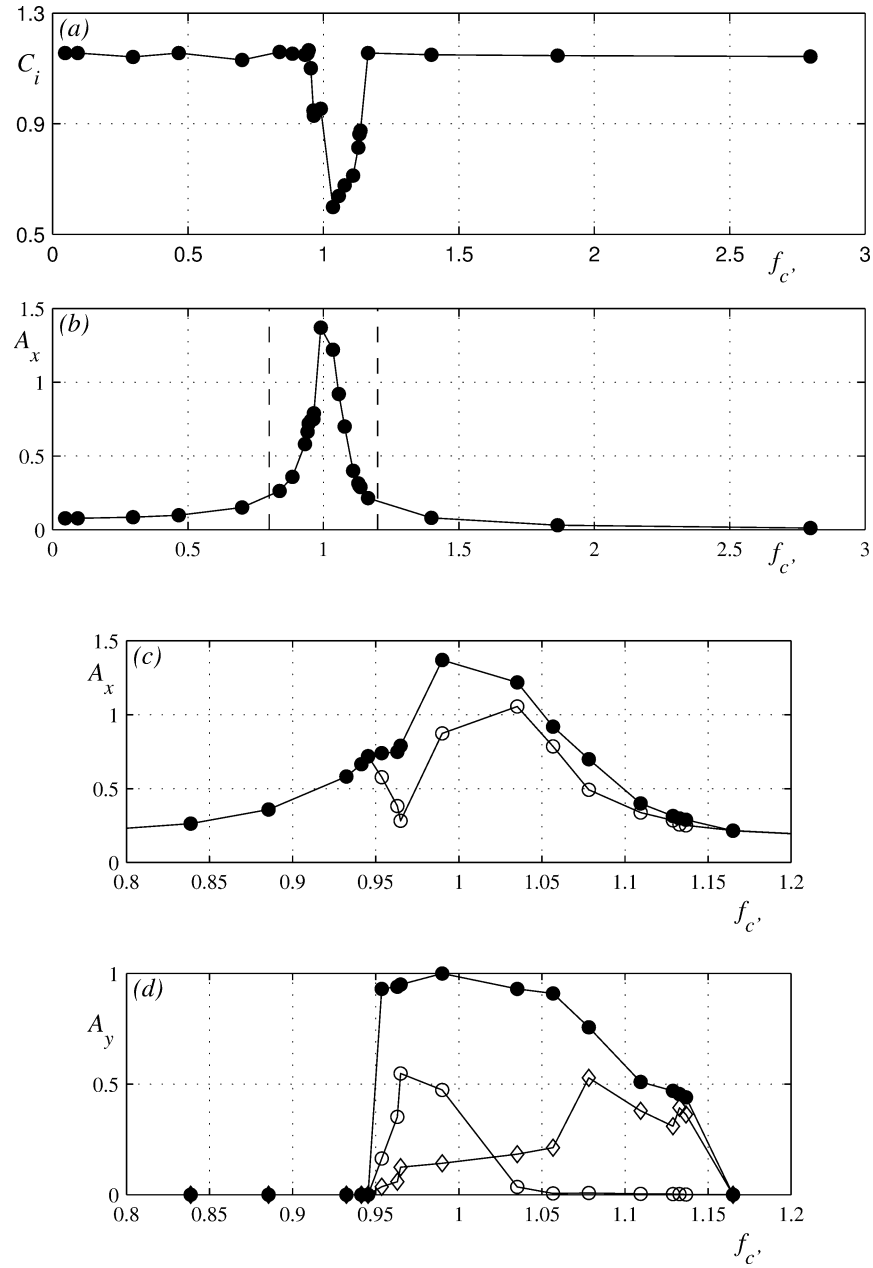

Fig. 5. Estimation of the C_i coefficient (a). Amplitude of the cylinder motion: (b) x-component, (c) x-component, (d) y-component. Total displacements A_x and A_y (•), contribution at the fundamental frequency A_{x0} and A_{y0} (∘), contribution at the natural frequency (⋄).

independent of $f_{c'}$ far from resonance condition, while for $f_{c'} \simeq 1$ a significant decreasing of C_i has been detected; such a diminution depends on the large oscillations, which modify the effective KC number relative to the body [6] and thus the added-mass effect. The amplitude A_x of the x-motion is reported in Fig. 5(b); it is easily estimated in the case of periodic solutions, being A_x equal to the contribution A_{x0} at the unitary frequency, in the nonperiodic regimes the reported is the maximum displacement detected during computation. The enlarged view, where the total amplitude A_x is plotted together with A_{x0}, confirms that the periodic–chaotic transition for $f_{c'} < 1$ is characterised by a decrease of the fundamental contribution; on the contrary, it remains dominant in the quasiperiodic and chaotic solutions with $f_{c'} > 1$, Fig. 5(c). When $f_{c'}$ is in the quasiperiodic range 1.129–1.137, the transversal amplitude A_y is greater than the in-line one, compare Fig. 5(d) with Fig. 5(c), and the contribution at the proper frequency is dominant; for $f_{c'} < 1$ the external frequency becomes the most significant,

as reported in Fig. 4(b). It must be pointed out that a stable periodic regime has been detected for values of A_x up to 0.72 for $f_{c'} < 1$, almost twice than the corresponding values for $f_{c'} > 1$. Such a difference can be partly justified by the value of the effective Keulegan–Carpenter number relative to the body; the loss of periodicity has been observed at values ranging between 1.5 and 1.7, the lowest value corresponds to $f_{c'} < 1$, the highest to $f_{c'} > 1$, diminishing the variability of the threshold condition.

The existence of quasiperiodic solutions can be related to the vorticity dynamics. The instantaneous vorticity fields in the case $f_{c'} = 1.133$ are reported in Fig. 6. At $t = 995$, Fig. 6(a), the cylinder has just reached an extremum of its trajectory, see Fig. 6(h), it has a small velocity and a significant acceleration. The vorticity field presents two nonsymmetric vortices of

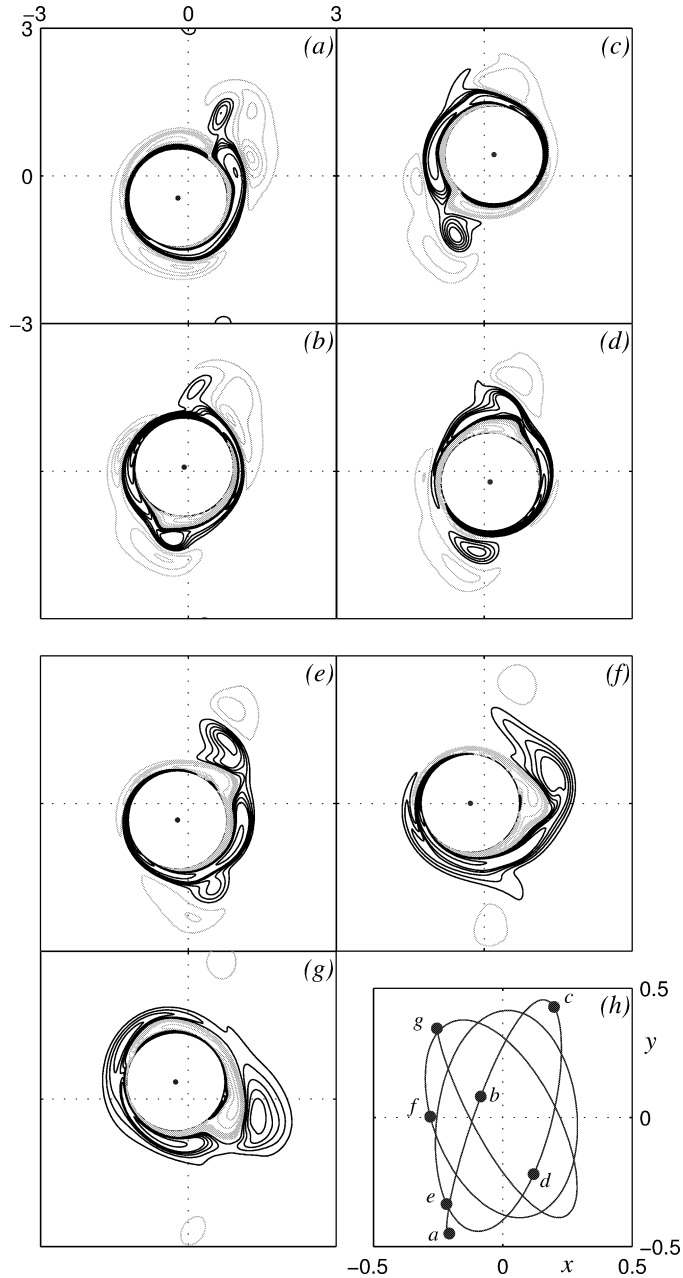

Fig. 6. Instantaneous vorticity fields in the fixed reference frame, $f_{c'} = 1.133$; $t = [495, 495.25, 495.5, 495.75, 496, 497, 498]$ from (a) to (g), respectively. Levels from 1 to 5 with step 1, from 10 to 70 with step 10 (black); symmetric negative values (grey). (h) cylinder trajectory from $t = 495$ to $t = 498$.

opposite sign separating at the rear side of the cylinder, with respect to the instantaneous direction of motion. In the upper-right portion of Fig. 6(a) a previously detached negative (clockwise) vortex can be observed. During the subsequent evolution, the cylinder movement induces a more intense separation of the positive vorticity layer, which develops on the body side external to the cylinder trajectory. The newly forming vorticity layers tend to detach the previously developed ones, Fig. 6(b); afterwards, the decelerating phase leads to the separation of a single positive vortex, lower-left portion of Fig. 6(c), which remains very close to the body, Fig. 6(d), merging eventually with the attached vorticity layer, Fig. 6(e). Some affinities can be observed between Figs. 6(a) and 6(e), depending on the similar positions of the cylinder along its trajectory at the corresponding times. More relevant differences can be observed in Fig. 6(f), and the completely different vorticity distribution of Fig. 6(g) is related to the reversed cylinder motion, Fig. 6(h). The dynamics can be summarised as follows: phases with significant relative velocity

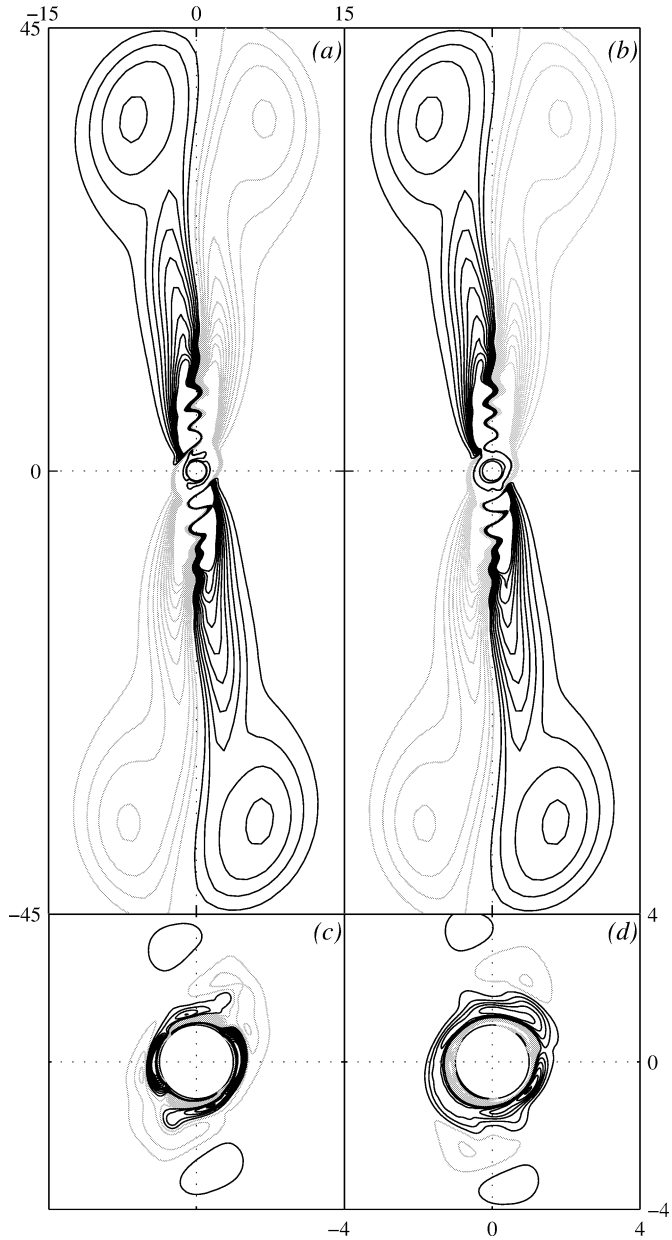

Fig. 7. Average vorticity fields, $f_{c'} = 1.133$; (a) and (c) period from $t = 495$ to $t = 496$, (b) and (d) period from $t = 496$ to $t = 497$. Contour levels: (a) and (b) from 0.005 to 0.05 with step 0.005 (black), and symmetric negative values (grey); (c) and (d) from 0.25 to 5.25 with step 0.25 (black), and symmetric negative values (grey).

are related to the development of the boundary-layer vortices, these detach and remain in the vicinity of the body during the decelerating stages. This behaviour has some similarities with that described by Cetiner and Rockwell [5] in the different context of a streamwise oscillating cylinder in a steady current; in such a problem, during the phases with highest velocities the formation of the von Karman vortices is observed, while the decelerating ones lead to a sort of frozen vorticity patterns. In the present case, the vortex formation has a similar dynamics, being driven by the body velocity; on the opposite, the frozen vorticity distribution has not been detected, depending on the orbital characteristics of the cylinder trajectory, which has different accelerating stages with the absence of effective zero-velocity positions.

A different description is given by the vorticity averaged over one period, Figs. 7(a) and 7(b) corresponding to two consecutive periods. Very low levels of the vorticity value have been selected in order to quantify the extension of the rotational part of the flow. No significant differences are observable far from the body; the similitude between the upper-right and lower-left negative vorticity distributions, similarly for the positive values, represents a typical effect of a periodic evolution. The lowest vorticity is due to the external forcing and it is almost unaffected by the cylinder motion, whose influence is confined near the body, Figs. 7(c) and 7(d). In Fig. 7(c) the mean field is characterised by two positive vorticity layers; they represent

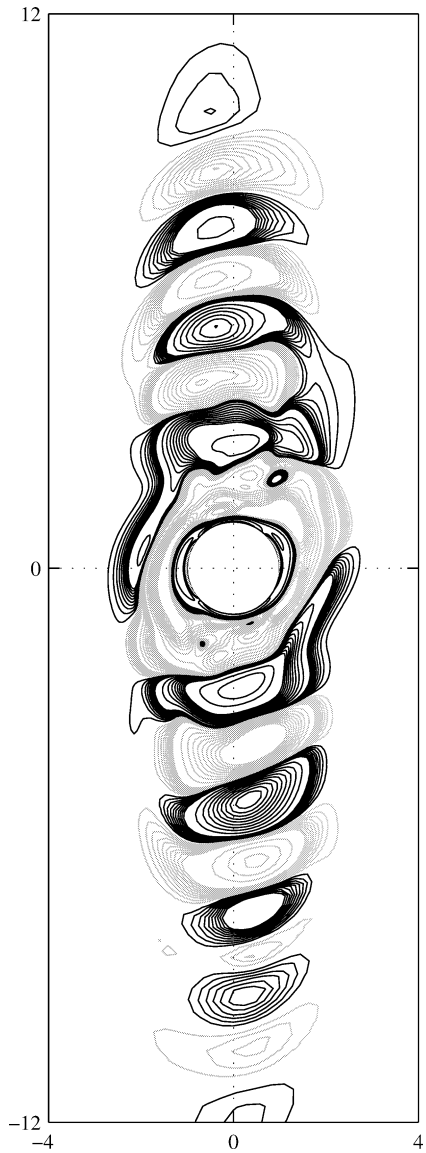

Fig. 8. Difference between the vorticity fields of Fig. 7. Contour levels: from 0.002 to 0.02 with step 0.002, from 0.02 to 0.2 with step 0.02, from 0.2 to 2 with step 0.2, from 5 to 20 with step 5 (black); symmetric negative values (grey).

the effect of the orbital motion of Fig. 6, where a dominance of the positive vorticity has been recognised. During the following period, the cylinder covers an orbit less inclined with respect to the x-axis, Fig. 6(h), with an enhanced persistence of the negative values. The positive vorticity is removed away from the body, which is completely surrounded by the negative one, Fig. 7(d).

The long-time influence of the detached vortices can be described by the difference between the mean fields of Fig. 7, reported in Fig. 8. Such a difference is significant close to the body and it is unappreciable far from it, clearly showing the dominant influence of the cylinder y-motion on the vorticity dynamics. The vorticity created during one period is not dissipated, but remains in the vicinity of the body interacting with the boundary-layer developing in the following periods. This interaction leads to a structure constituted by several alternate vortices, seven in the upper portion of the figure, eighth in the lower one. The structure is related to the timescale $T_p = (f_{c'} - 1)^{-1} \simeq 7.53$, which is constructed from the two competing frequencies. The quasiperiodicity of the solution is therefore an intrinsic property of the vorticity field, whose integral representation is given by the cylinder motion. A similar structure has been observed in all the cases with a stable quasiperiodic regime.

Close to the resonance, the x-component of the cylinder motion becomes again dominant, see Fig. 5. The growth of KC relative to the body gives a more complex dynamics of the vorticity field. During each period of the external stream, the birth, development, and final ejection of several intense vortices can be observed, with a strong interaction with those previously detached. Such compact vortex structures tend to remain in the vicinity of the body, enhancing or inhibiting the development of the boundary-layer. The interaction between a large number of vortices gives an unpredictable evolution of the forces acting on the body, inducing the transition to a chaotic solution. As an example, the instantaneous vorticity fields during a period of the external stream are reported in Fig. 9, for $f_{c'} = 1.035$. During this phase, the almost rectilinear trajectory covers a flat knot, Fig. 9(f), being dominant the x-component of the body motion. At the instants of time with maxima of the relative velocity,

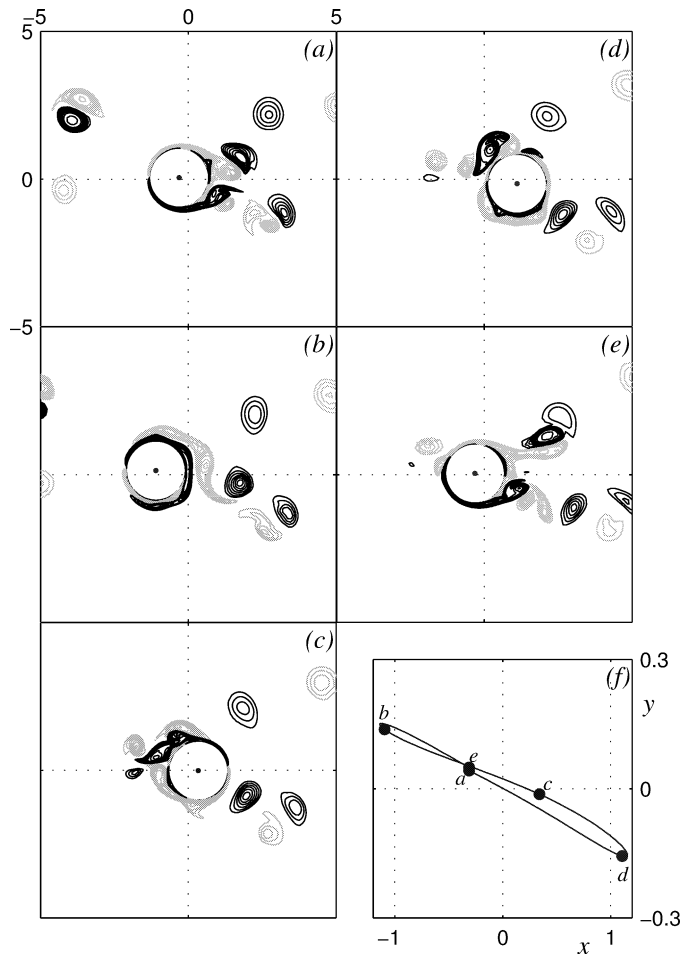

Fig. 9. Instantaneous vorticity fields in the fixed reference frame, $f_{c'} = 1.035$; t from 495 to 496, step 0.25, from (a) to (e), respectively. Levels from 2 to 20 with step 2, from 20 to 70 with step 10 (black), and symmetric negative values (grey); (f) cylinder trajectory.

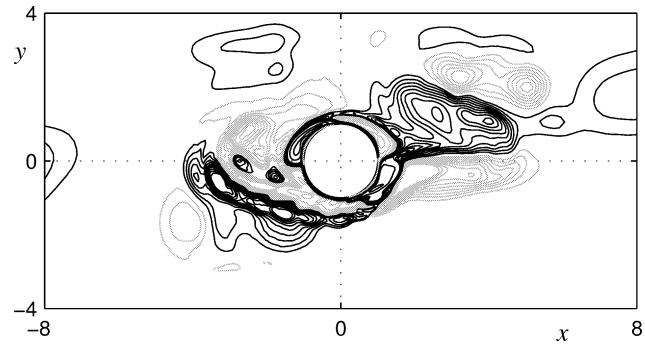

Fig. 10. Difference between average vorticity fields, (two consecutive periods) $f_{c'} = 1.035$. Contour levels: from 0.3 to 3 with step 0.3, from 3 to 21 with step 3 (black), and symmetric negative values (grey).

Figs. 9(a), 9(c) and 9(e), we can observe two forming vortices, which tends to couple with the previously ejected of opposite sign. During the decelerating phases the attached vortices tends to depart from the body forming new freely moving ones, Figs. 9(b) and 9(d). Any trace of regular evolution cannot be found; the unpredictability of the system behaviour is suggested by the fixed cylinder case results (see, for example, [10]), where an enhanced complexity of the forces signal is found increasing *KC*. The present case gives a Keulegan–Carpenter number relative to the body approximately equal to 4, corresponding to the regime *E* in the fixed body case [2]. Some affinities can be observed, but a relevant difference is represented by the size of the detached vortices: in the fixed case they are comparable with the body dimension, while in the present one more compact structures have been found.

The analysis of the average fields confirms the relationship between the vorticity dynamics and the characteristics of the body motion. The difference between two consecutive mean fields at $f_{c'} = 1.035$ is plotted in Fig. 10, showing the dominance of the in-line motion. As previously observed in the quasiperiodic case, the influence of the body motion is significant in a limited portion of the flow domain, while far from the cylinder the vorticity distribution is dominated by the periodic effects due to the external forcing. The mean vorticity fields close to the body have a complex distribution, with the absence of any sort of structure, compare with Fig. 8, giving rise to the observed chaotic motion of the cylinder.

4. Conclusion

The coupled dynamics of an elastically mounted cylinder immersed in a sinusoidal stream has been analysed. The flow parameters have been selected in correspondence of a periodic solution of the fixed body case, the problem has been studied varying the properties of the cylinder-constraints system, here modelled as a simple oscillator with two degrees of freedom. The solution has been obtained by the numerical integration of the two-dimensional Navier–Stokes equations in the vorticity-streamfunction formulation coupled with the body equations of motion.

An important dependence of the cylinder motion on the characteristics of the oscillator has been found, with a periodic behaviour far from the resonance condition. Approaching this, the loss of symmetry and the appearance of significant transversal motion have been detected. A chaotic regime is found in a range around resonance which confines directly to the periodic state on one side, when the elastic frequency is smaller than the forcing one, while a transition through quasiperiodicity, given by the competition of the natural and external frequencies of the system, is found on the opposite side. The concomitance of symmetry and periodicity losses evidences a strong fluid–structure interaction: between the phenomena driven by the forcing stream, characterised by the fundamental frequency, and those related to the cylinder motion, at the natural frequency of the oscillator; the nonlinearity of such an interaction does not allow the easy identification of the single effects.

The analysis of the vorticity field has shown a relationship between the observed body motion and the presence of several free wake vortices with a very slow dissipating dynamics. The transition to a chaotic regime of motion has shown that the interaction between a stream and an elastically constrained body has a very complex behaviour, even with values of the flow parameters giving a stable periodic and symmetric solution, which can not be modelled with simplified schemes or derived from the known results of the fixed body case. The very long time required by the transition to manifest itself, which has been detected in some cases, represents a remarkable result; it can give some suggestions for the study of similar problems, showing the necessity of an extended analysis in order to capture the experimentally observed phenomena. In conclusion, even at moderately low values of the Keulegan–Carpenter number, resonance gives rise to complex, unpredictable, phenomena which should be avoided in practical applications.

The present case of an elastically moving cylinder is a simple model of the fluid–structure interaction, which also represents a preliminary scheme for several applied problems. Despite its simplicity, the calculated results show an important mutual interaction between the body and the fluid motion. Extensions to different elastic behaviours, realistic structural damping, or to different cylindrical shapes, should be included for reliable modelling of specific applied conditions where interaction is expected to develop. The assumption of two-dimensional flow does not affect qualitatively the results in the range of fluid parameters here analysed; however, it must be taken in account at higher values of the Keulegan–Carpenter number when the flow develops three-dimensional instabilities.

Acknowledgement

The author is grateful to Gianni Pedrizzetti for helpful comments and suggestions.

References

[1] C.H.K. Williamson, Sinusoidal flow relative to circular cylinders, J. Fluid Mech. 155 (1985) 141–174.
[2] M. Tatsuno, P.W. Bearman, A visual study of the flow around an oscillating circular cylinder at low Keulegan–Carpenter numbers and low Stokes numbers, J. Fluid Mech. 211 (1990) 157–182.
[3] H. Honji, Streaked flow around an oscillating circular cylinder, J. Fluid Mech. 107 (1981) 509–520.
[4] T. Sarpkaya, Force on a circular cylinder in viscous oscillatory flow at low Keulegan–Carpenter numbers, J. Fluid Mech. 165 (1986) 61–71.
[5] O. Cetiner, D. Rockwell, Streamwise oscillations of a cylinder in a steady current. Part 1. Locked-on states of vortex formation, J. Fluid Mech. 427 (2001) 1–28.
[6] P. Anagnostopoulos, G. Iliadis, Numerical study of the flow pattern and the in-line response of a flexible cylinder in an oscillatory flow, J. Fluids Struct. 12 (1998) 225–258.
[7] P. Hall, On the stability of the unsteady boundary layer on a cylinder oscillating transversely in a viscous fluid, J. Fluid Mech. 146 (1984) 347–367.
[8] X. Lu, C. Dalton, J. Zhang, Application of large eddy simulation to an oscillating flow past a circular cylinder, J. Fluids Eng.-ASME 119 (1997) 519–525.
[9] J. Zhang, C. Dalton, The onset of three-dimensionality in an oscillating flow past a fixed circular cylinder, Internat. J. Numer. Methods Fluids 30 (1999) 19–42.
[10] P. Justesen, A numerical study of oscillating flow around a circular cylinder, J. Fluid Mech. 222 (1991) 157–196.
[11] G. Vittori, P. Blondeaux, Quasiperiodicity and phase locking route to chaos in the 2-D oscillatory flow around a circular cylinder, Phys. Fluids 5 (1993) 1866–1868.
[12] R. Panton, Incompressible Flow, Wiley, New York, 1996.
[13] C.A. Fletcher, Computational Techniques for Fluid Dynamics I, Springer-Verlag, Berlin, 1988.
[14] J.H. Williamson, Low-storage Runge–Kutta schemes, J. Comp. Phys. 35 (1980) 48–56.
[15] C. Canuto, M.Y. Hussaini, A. Quarteroni, T.A. Zang, Spectral Methods in Fluid Dynamics, Springer-Verlag, New York, 1988.
[16] A. Pentek, J.B. Kadtke, G. Pedrizzetti, Dynamical control for capturing vortices near bluff bodies, Phys. Rev. E 58 (1998) 1883–1898.